Supporting Information: Crystal Structure Influences Migration Along Li and Mg Surfaces

Ingeborg Treu Røe, Sverre M. Selbach, and Sondre Kvalvåg Schnell*

Department of Materials Science and Engineering, Norwegian University of Science and Technology, NTNU, Trondheim, Norway

E-mail: sondre.k.schnell@ntnu.no

Simulation details

The density functional theory (DFT) calculations were performed with the Vienna *ab initio* Simulation Package (VASP)[S1,S2] and the Li_sv and Mg projector augmented wave (PAW)[S3] pseudopotentials supplied with VASP.5.4. Plane waves were expanded up to cutoff energies of 500 eV for Li and 350 eV for Mg and the PBEsol functional was used.[S4] The bcc, fcc and hcp bulk structures of Li and Mg are relaxed to within 1 meV/Å. The obtained lattice constants are given in Tab. S1.

Table S1: The lattice constants of the Li and Mg bulk structures

		bcc (Å)	fcc (Å)	hcp (Å)
Lithium	PBEsol	3.42	4.30	a=3.06 c=4.90
	Exp.	3.51[S5]		a=3.11[S6] c=5.09[S6]
	PBE	3.44[S7,S8]	4.33[S7]	a=3.06[S7] c=5.00[S7]
Magnesium	PBEsol (A)	3.55	4.49	a=3.16 c=5.22
	Exp.			a=3.21[S9,S10] c=5.21[S9,S10]
	PBE			a=3.19[S8] c=5.18[S8]

The migration energy barriers (MEBs) are found using the Nudged Elastic Band (NEB) method implemented in VASP by Henkelman *et al.*[S11–S14] The NEB calculations are carried out on supercells exposing different surfaces of the bcc, fcc and hcp structures, and with dimensions exceeding 12 Å in all directions and an additional 15 Å of vacuum in the z-direction. This corresponds to a 4x4 or 5x5 geometry in the xy-plane, and more than 8 layers in the z-direction, as shown in Fig. S1 for Li bcc (001). Five images are used in the NEB calculations with a spring constant of 5 eV/Å between them, and the max force in each image has converged to less then 10 meV/Å.

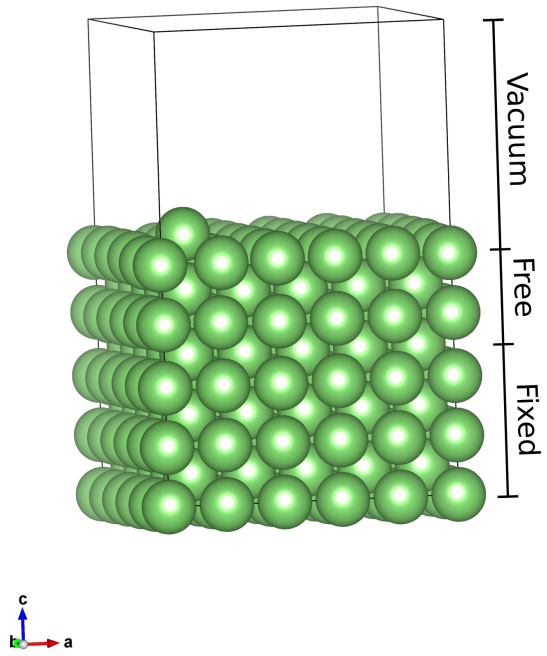

Figure S1: The supercell of Li bcc (001), indicating the vacuum, and the free and fixed layers.

Convergence testing

Convergence testing on the supercells were performed to ensure a "correct" behaviour of the surface. The atoms in the four uppermost layers of the supercells were allowed to move freely, while the rest of the atoms were fixed in space, mimicking the bulk in a real crystal. The convergence of the atomic positions of the free layers are shown in Fig. S2 as a function of total number of layers in the supercell.

In addition to the number of layers in the supercell, the extent of the xy-plane is important for realistic MEBs. If the surface is too small, the migrating atom will feel itself across the periodic boundaries, and thus affect the MEBs. Figure S3 shows the dependence of the MEB on the xy-plane area for the minimum energy path on Li bcc (001).

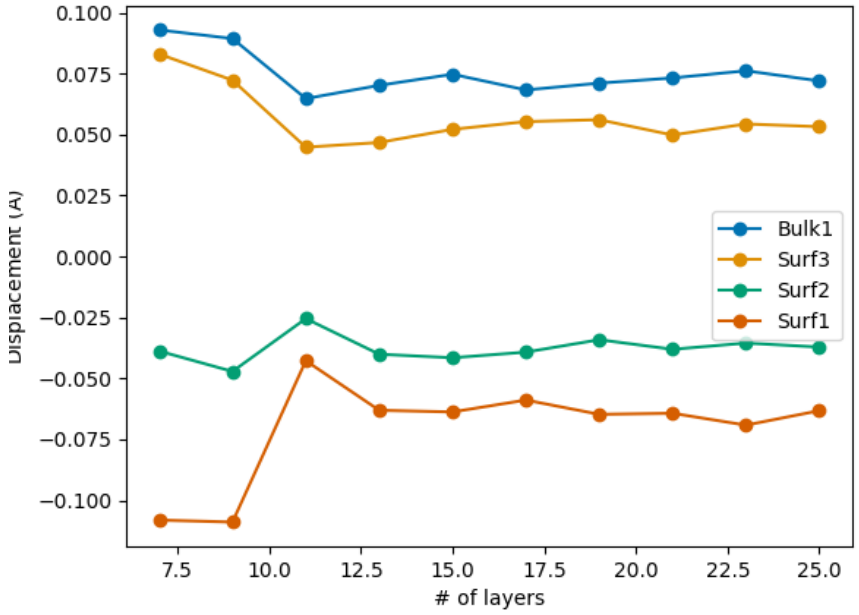

Figure S2: The displacement of the different layers within a Li bcc (001) supercell as a function of the total number of layers. Bulk1 labels the first free layer, and Surf1 the uppermost layer interfacing to vacuum.

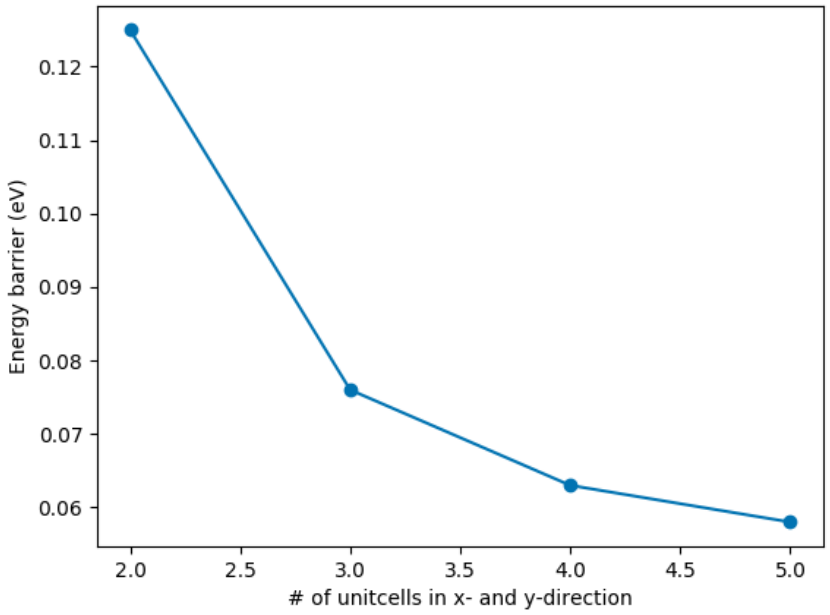

Figure S3: The migration energy barrier of the minimum energy path as a function of number of unit cells in one direction of the Li bcc (001)

Comparison to literature

The MEB of the 2x2-geometry of the Li bcc(001) (Fig. S3) corresponds well with the reported values of Jäckle *et al.*,[S8] but is not converged with respect to the xy-dimension. However, the results herein correspond to the MEBs found by Gaissmaier *et al.*[S15] A comparison of the MEBs of the Li bcc facets from the present study, Gaissmaier *et al.* and Jäckle *et al.* is found in Fig. S4. In addition, the MEB of the bcc (111) surface for both the present and Gaissmaier *et al.*'s work deviates from Jäckle *et al.*. A likely explanation is that we found the exchange mechanism to have smaller MEB, while Jäckle *et al.* have calculated the MEB of the bcc (111) surface based on the adsorption energies (thus, for a hopping mechanism).

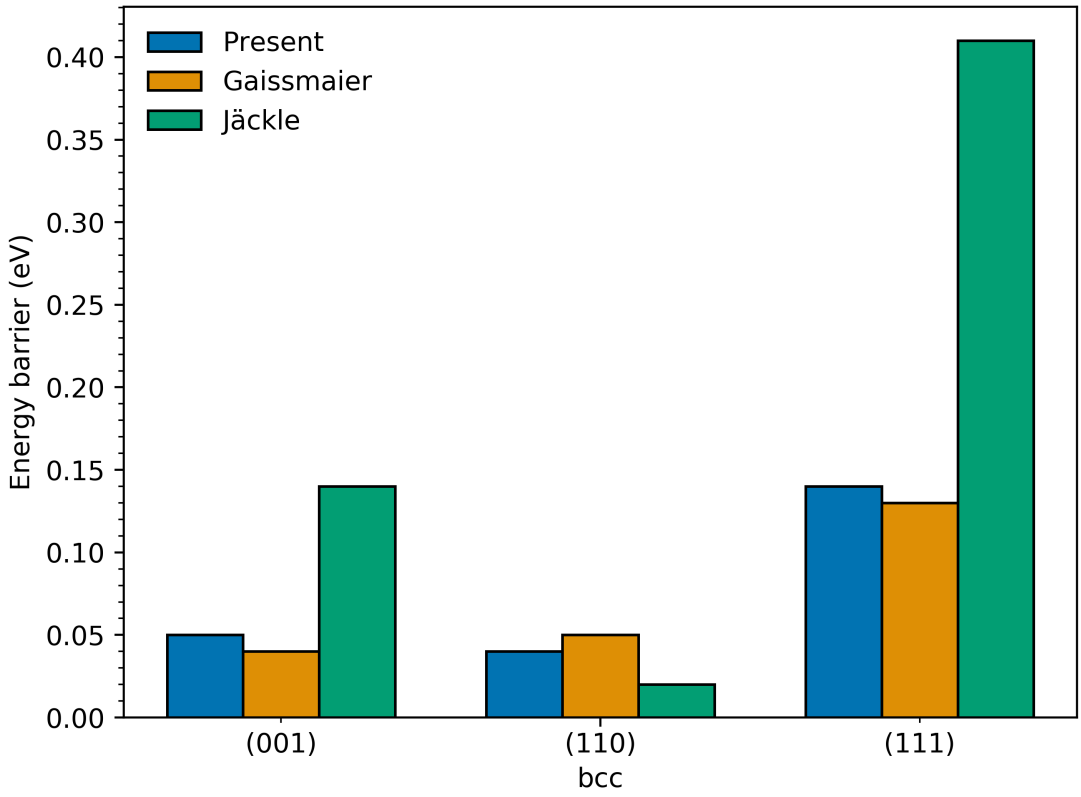

Figure S4: The MEB of the Li bcc facets calculated in the present study compared to Gaissmaier *et al.*[S7] and Jäckle *et al.*[S8]

Surface Energy Calculations and Adaptive Common Neighbour Analysis

The surface energies of the different facets were calculated using:

$$E_{surf} = \frac{E_{slab} - nE_{bulk}}{2A} \tag{S1}$$

where E_{slab} is the energy of the slab, E_{bulk} is the energy of the bulk per atom, n is the number of atoms in the slab and A is the surface area. The obtained surface energies are displayed in Tab. S2.

Table S2: The surface energies of the different facets of the Li and Mg structures

Crystal structure	Surface	Lithium (J/m^2)	Magnesium (J/m^2)
bcc	001	0.49	0.74
	110	0.53	0.63
	111	0.57	0.82
fcc	001	0.50	0.74
	110	0.55	0.74
	111	0.54	0.54
hcp	0001	0.54	0.56
	10-11	0.60	0.82

The adaptive common neighbour analysis (cna) was performed using Ovito.[S16] Tab. S3 shows the number of atoms in a supercell that has changed its structure from the stable position to the saddle point, normalized over the number of atoms that are free to move. A positive number means that the atoms in the saddle point structure has changed their structure to something different than the bulk. Oppositely, a negative result signifies that the atoms of the stable position was recognized in a different structure, and changed to the bulk structure at the saddle point.

Table S3: The difference in local structure between the stable position and the saddle point for different migration paths at the Li and Mg facets normalized over the number of atoms in the slab that is free to move

		Lithium (%)	Magnesium (%)
bcc	001	4	4
	110	0	0
	111	9	0
fcc	001	7	0
	110	6	0
	110[a]	-23	0
	111	0	0
hcp	0001	0	0
	10-11		

[a]Not the minimum energy path

Density of States Calulations

The electronic density of states (DOS) was investigated for the stable and saddle positions for every migration path using VASP. The resulting DOS of the stable and saddle positions of the minimum energy path on the bcc (001) surface for Li and Mg is shown in Fig. S5. Based on the DOSes, the difference between the stable and saddle position was calculated with:

$$\Delta DOS = \sqrt{\sum_{E} (dos_{E,stable} - dos_{E,saddle})^2} \tag{S2}$$

where $dos_{E,i}$ is the density of states at energy E, normalized with respect to the Fermi energy, of position i (*i.e.* the stable or saddle position). The ΔDOS was calculated for two different energy ranges; one summed over the valence band, termed 'vDOS', up to the Fermi energy, and one over the s- and p-bands, termed 'all'.

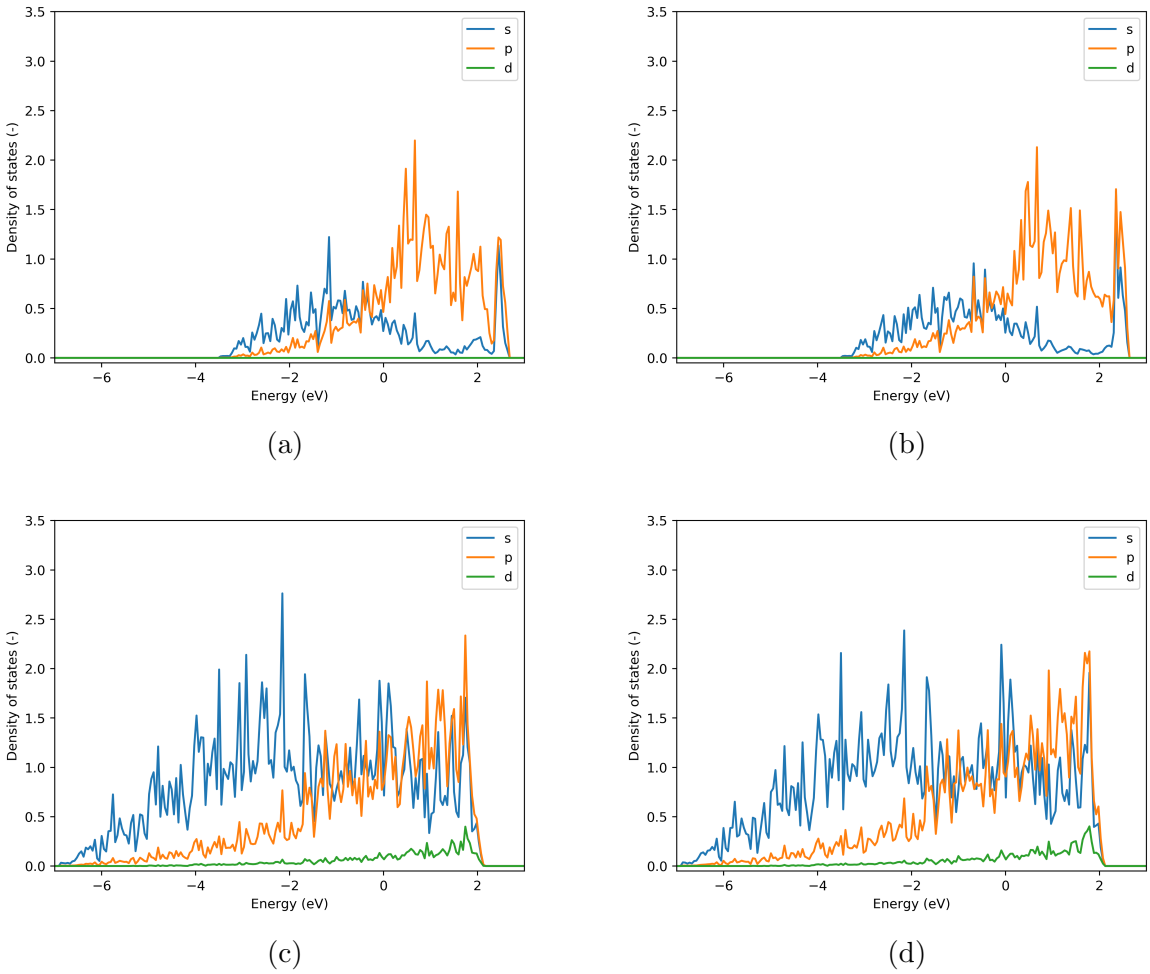

Figure S5: The DOS of a) and c) the stable, and b) and d) saddle position of the minimum energy path on the Li (a) and b)) and Mg (c) and d)) bcc (001) surface

References

(S1) Kresse, G.; Furthmüller, J. Efficiency of ab-initio total energy calculations for metals and semiconductors using a plane-wave basis set. *Computational Materials Science* **1996**, *6*, 15–50.

(S2) Kresse, G.; Joubert, D. From ultrasoft pseudopotentials to the projector augmented-wave method. *Physical Review B* **1999**, *59*, 1758–1775.

(S3) Blöchl, P. E. Projector augmented-wave method. *Physical Review B* **1994**, *50*, 17953.

(S4) Perdew, J. P.; Ruzsinszky, A.; Csonka, G. I.; Vydrov, O. A.; Scuseria, G. E.; Constantin, L. A.; Zhou, X.; Burke, K. Restoring the Density-Gradient Expansion for Exchange in Solids and Surfaces. *Physical Review Letters* **2008**, *100*, 136406.

(S5) Kellington, S. H.; Loveridge, D.; Titman, J. M. The lattice parameters of some alloys of lithium. *Journal of Physics D: Applied Physics* **1969**, *2*, 1162.

(S6) Barrett, C. S. X-ray study of the alkali metals at low temperatures. *Acta Crystallographica* **1956**, *9*, 671–677.

(S7) Gaissmaier, D.; Fantauzzi, D.; Jacob, T. First principles studies of self-diffusion processes on metallic lithium surfaces. *The Journal of Chemical Physics* **2019**, *150*, 41723.

(S8) Jäckle, M.; Groß, A. Microscopic properties of lithium, sodium, and magnesium battery anode materials related to possible dendrite growth. *The Journal of Chemical Physics* **2014**, *141*, 174710.

(S9) Baraille, I.; Pouchan, C.; Causà, M.; Marinelli, F. Comparison between Hartree-Fock and Kohn-Sham electronic and structural properties for hexagonal-close-packed magnesium. *Journal of Physics Condensed Matter* **1998**, *10*, 10969–10977.

(S10) Clendenen, G. L.; Drickamer, H. G. Effect of Pressure on the Volume and Lattice Parameters of Magnesium*. *Physical Review* **1964**, *135*, A 1643.

(S11) Henkelman, G.; Jónsson, H. Improved tangent estimate in the nudged elastic band method for finding minimum energy paths and saddle points. *Journal of Chemical Physics* **2000**, *113*, 9978.

(S12) Henkelman, G.; Uberuaga, B. P.; Jónsson, H.; Jó, H. A climbing image nudged elastic band method for finding saddle points and minimum energy paths. *The Journal of Chemical Physics* **2000**, *113*, 214106.

(S13) Jonsson, H.; Mills, G.; Jacobsen, K. W. Nudged elastic band method for finding minimum energy paths of transitions. *Classical and Quantum Dynamics in Condensed Phase Simulations - Proceedings of the International School of Physics* **1998**, 385–404.

(S14) Sheppard, D.; Xiao, P.; Chemelewski, W.; Johnson, D. D.; Henkelman, G. A generalized solid-state nudged elastic band method. *The Journal of Chemical Physics* **2012**, *136*, 74103.

(S15) Gaissmaier, D.; Borg, M.; Fantauzzi, D.; Jacob, T. Microscopic Properties of Na and Li—A First Principle Study of Metal Battery Anode Materials. *ChemSusChem* **2020**, *13*, 1–14.

(S16) Stukowski, A. Visualization and analysis of atomistic simulation data with OVITO–the Open Visualization Tool. *Modelling and Simulation in Materials Science and Engineering* **2010**, *18*, 015012.